JOURNAL OF COMMUNICATION AND INFORMATION SYSTEMS, VOL. 36, NO.1, 2021.

75

Coupling Impact Between a Radial Antenna and Guided Modes on Twisted-Pair Systems Operating in Millimeter-Wave

Brenda P. T. Sousa, Daynara D. Souza, Gilvan S. Borges, Roberto M. Rodrigues, André M. Cavalcante and João C. W. A. Costa

Abstract—**Recent research points out that transmission at terabits per second (Tbps) is feasible over copper cables if they were used as millimeter waveguides. The challenge is how to efficiently couple signals to the higher-order modes of twisted-pairs. This paper investigates the effectiveness of radial antennas on the coupling of near-terahertz signals to twisted-pairs. For that, the scattering parameter of the proposed antenna and the intensity of the electric field around the pairs are evaluated from numerical simulations. We also present the attenuation coefficients of four guided modes in a twisted-pair with typical constructive parameters and evaluate aggregate data rate results through Shannon's capacity. The results indicate the coupling efficiency may reach up to 71.62%, yielding an aggregate data rate over copper cables up to 0.17 Tbps at 10 m.**

Index Terms—**Antennas, Coupling of guided modes, Terabit DSL, Twisted-pair.**

I. INTRODUCTION

BROADBAND systems that use copper cables like DSL (Digital Subscriber Line) exploit the TEM (Transverse Electromagnetic) mode to transmit data. However, to ensure higher rates it is necessary to use increasing frequency bands, where the attenuation over the TEM is higher. So the way to achieve higher data rates is to limit the range of the system as one goes up in frequency [1], [2]. As applications for 5G systems require rates above tens of Gbps (Gigabit per second) [3], the use of TEM mode on wired systems makes it unfeasible to achieve such high rates, even for short links.

In order to give more survival to cables in the context of 5G applications, it was proposed to explore the transmission of higher-order propagation modes for transmission, in a system

B. P. T. Sousa and D. D. Souza are with the Federal University of Pará - UFPA, Belém, PA, 66075-110 Brazil. e-mail:{brenda.ppenedo,daynaradiassouza}@gmail.com.

G. S. Borges is with Federal Institute of Pará - IFPA, Belém, PA, 66093-020 Brazil. e-mail: gilvan.borges@ifpa.edu.br.

R. M. Rodrigues is with Electrical and Biomedical Engineering Faculty, Federal University of Pará - UFPA, Belém, PA, 66075-110 Brazil. e-mail: rmr@ufpa.br.

A. M. Cavalcante is with Ericsson Research Brazil, Indaiatuba, SP, 13337-300 Brazil. e-mail: andre.mendes.cavalcante@ericsson.com.

J. C. W. A. Costa is with Computer and Telecommunications Engineering Faculty, Federal University of Pará - UFPA, Belém, PA, 66075-110 Brazil. e-mail: joaoweyl@gmail.com.

called Terabit DSL [4]. These modes are of type TE (Transverse Electric) or TM (Transverse Magnetic) and arise when the wavelengths associated with the operating frequencies are of the same order or smaller than the dimensions of the cross-section of the cable, which comprises the millimeter-wave frequency range [4], [5]. Through those modes, one can achieve data rates of up to 1 Tbps in a single twisted-pair of 100 m, according to [4]. Despite its potential, there are two issues related to the predictions reported in [4], that causes an evident overestimation of the performance of Terabit DSL.

The first one regards the model assumed by [4] for the cable's attenuation: the Sommerfeld line. It is a single bare-wire model that does not describe twisted-pairs suitably. Simulations to determine the data rate of the Terabit DSL system considering the attenuation of the twisted-pair cable with realistic constructive characteristics are done in [6], where it was indicated that the data rate and range of the pair do not reach the levels presented in [4], but are much higher than those of the last generation of DSL. In [7], [8], the propagation properties of a cable structure close to telephone cables are measured, at the frequency of 200 GHz, but this measured waveguide lacks typical characteristics of twisted-pairs, such as its twisting and isolation.

The second one is the assumption in [4] that all power delivered to the twisted-pairs is coupled to the higher-order modes, i.e., it is assumed perfect coupling. In contrast, the efficient excitation of such modes (high coupling efficiency) is a big challenge. Even for simple structures as the Sommerfeld waveguide, there are still limitations to efficiently couple near-THz signals [9]. The work [6] also assumes perfect coupling and does not investigate which structures would be viable for excitation and coupling of the higher modes.

The goal of the paper is to investigate the coupling between an excitation source formed by a radial antenna and a twisted-pair. Here, differently from [4], [6], [8], we investigate the transmission capacity when using the higher-order guided modes of a twisted-pair, considering both the attenuation effects of the modes and the structures used for excitation and coupling.

The contributions of this paper are: i) present attenuation values of the higher-order modes of twisted-pairs with typical physical characteristics, ii) evaluate the radial antenna structure, the positioning of the twisted-pair, and the frequency range that maximizes the coupling efficiency, iii) estimate data rate from the observed coupling efficiency and attenuation

results, iv) present a more realistic performance of using the higher-order modes of twisted-pair and compare with those reported in previous works.

The remainder of this paper is organized as follows. Section II describes the features of the higher-order modes of twisted-pairs and different coupling methods. Section III presents the methodology of the study employing numerical simulations and the approach to calculate data rates. Section IV presents results concerning the coupling efficiency, and data rates assuming the observed coupling efficiency. Finally, Section V presents our conclusions.

II. PROPAGATING AND COUPLING SIGNALS TO GUIDED MODES

A. Waveguides

The use of twisted-pair as a waveguide is still not a very explored topic. However, waveguides made up of simpler cylindrical conductors and which already have well-established analytical modeling, help to understand and evaluate the guidance in the twisted-pair. Among these simpler waveguides, we can mention Sommerfeld and Goubau waveguides. These are also known as surface waveguides, since electromagnetic fields are guided on the surfaces of their conductors along their lengths [10].

Sommerfeld's waveguide is described by a bare cylindrical conductor, as shown in Fig. 1 a. The possibility of guiding along the surface of a conductor was demonstrated by Sommerfeld, with this structure, in 1899. It was shown that the main mode of propagation in the bare conductor is a TM mode with no cutoff frequency and that its existence is only when conductor conductivity (σ) is finite [11].
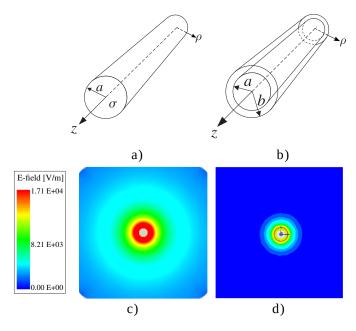

Fig. 1. Waveguides a) Sommerfeld and b) Goubau. Distribution of electric field around the guides of c) Sommerfeld and d) Goubau.

Despite the advantage of low attenuation along the conductor, Sommerfeld demonstrated that this bare conductor guided the propagated wave in a dispersed way, in other
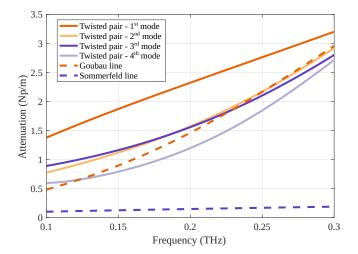

Fig. 2. Attenuation level of Sommerfeld, Goubau and twisted-pair waveguides.

words, it extended over a wide area around the conductor before decaying to negligible values, making the guide very susceptible to external disturbances, imperfections and curves in the guide, shown in Fig.1c [11] [12].

Solving the field dispersion problem on the Sommerfeld line, we have the Goubau waveguide [12]. This waveguide is a bare conductor with the addition of a dielectric coating around the cylindrical conductor, as shown in Fig. 1b. The presence of the dielectric causes the electromagnetic field guided on the surface to approach the conductor, that is, it increases the confinement of the field to the structure, as shown in Fig. 1d.

Thus, the Terabit DSL scenario sees the possibility of using the twisted-pair as a waveguide, as well as these simpler guides by Sommerfeld and Goubau. This possibility of using the twisted-pair as a waveguide is shown in [6], due to the attenuation level of the twisted-pair, as shown in Fig. 2, that is approximated to the level of the Goubau waveguide.

The distribution of electric field in Fig. 1 and the attenuation in Fig. 2 was calculated using the software HFSS (High-Frequency Structure Simulator), following the same procedure as [6]. It was assumed a 0.255 mm copper radius and 0.4 mm polyethylene insulation radius. The materials were configured to have a conductivity equal to $5.8 \times 10^7 S/m$ for copper. The dielectrics loss tangent and relative permittivity are 4×10^{-4} in 10 GHz and 2.25 for polyethylene, according to the values presented in [13].

B. Antennas and Coupling Method

Despite the possibility of using the twisted-pair as a waveguide, in the literature there is no study that makes the study of which excitation source and which coupling method would be more suitable for such activity.

In the context of surface waves and cylindrical waveguides, the literature points out that the most appropriate is the use of antennas that propagate waves with circular polarization. This recommendation is due to the difficulty of coupling a linearly polarized source in radial structures, which happens due to

the weak spatial overlap of the guided mode that is radially polarized [9].

Thus, in the literature, in addition to the use of antennas with radial polarization, there are alternatives to facilitate coupling in waveguides, for example, using methods that increase efficiency between the antenna and the waveguide in GHz to THz bands.

Among these coupling methods, the literature includes the scattering in-couple [14], mode filters [15], plasmonic in-couplers [16] and the used method in this article lens focusing [17]. In the scattering in-couple method, a linearly polarized THz pulses are generated by a coupled fiber photoconductive transmitter and focused on a stainless steel waveguide. A second stainless steel wire acts as an input coupler. Thus, a radially polarized mode is excited in the space around the waveguide [14]. The Mode filters method consists of using a differential phase plate that induces a polarization inversion in comparison to the electromagnetic field previously launched in the wire [15]. The plasmonic in-couplers method involves the insertion of the end of a tapered metal wire in the center of a circular opening smaller than the wavelength, made in an autonomous planar metallic sheet [16]. The opening of the shortest wavelength is surrounded by concentric annular grooves. Finally, the lens focusing method consists of using a lens for directly focusing a broadband THz wave beam with conventional lenses [17].

Among these methods used in the literature, there are very varied efficiencies, also due to the different scenarios that are used. These values can be seen in Table I. As shown in the table, we chose the method that has higher efficiency, the lens focusing method.
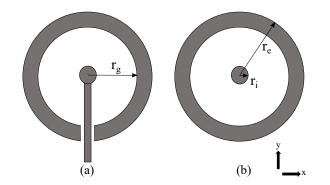

Fig. 3. Model of the photoconductive antenna proposed in [9]. (a) Real model with feeding rod. (b) Ideal model used for simulation.
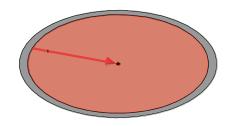

Fig. 4. Lumped port used to fed the antenna, from HFSS.

TABLE I
COUPLING EFFICIENCY FOR EACH METHOD.

Work	Method	Efficiency
[14]	Scattering in-couple	0.50%
[15]	Mode filters	50%
[16]	Plasmonic in-couplers	Unspecified
[17]	Lens focusing	66.30%

III. SIMULATION SETUP

A. Construction of the Simulation Scenario

The simulation scenario was built using the software HFSS, which uses the finite element method for computational solutions for electromagnetic design and analysis.

The assembly of the 3D scenario was organized and simulated in the following steps: construction of the antenna, attachment of the antenna to the coupling lens and substrate, assembly of the cable as a waveguide, and positioning of it in the scenario.

1) Antenna, Substrate and Lens: The antenna used in this article was based on an antenna proposed in [9], as mentioned in Section II-B, it has radial polarization and good coupling with radial structures in the THz range, such as metal wire waveguides, similar to the Terabit DSL scenario. The combination of the antenna and coupling method (radial antenna plus dome) of [9] matched very well physically and

electromagnetically. Thus, we chose to use it, since another efficient set of antennas and coupling methods was not known and would require further investigation. As shown in Fig. 3, the antenna consists of two electrodes, the outer one with radius r_e, and the inner one with radius r_i. The actual antenna is fed by an electrode that crosses the outer electrode and reaches the inner electrode, as shown in Fig. 3a. However, for simulation purposes, the antenna was mounted without this feeding electrode, being excited in the area between the ring electrodes (gap) using a lumped port available in the software, shown in Fig 4. The red area represents the lumped port and the arrow the direction of excitation (from the external electrode to the internal).

As presented in [9], the proposed antenna is used with two structures to improve coupling on the waveguide: a substrate and a coupler lens (or dome). The antenna used was arranged in the x-y plane between the substrate and lens interface, as outlined in Fig. 5.

The antenna proposed in [9] has dimensions described in Table II. In [9] the substrate consists of a medium with a dielectric constant equivalent to 13, which is approximately equal to the GaAs (Gallium Arsenide) material, with a thickness of 500 μm. The coupler lens is represented by a 2000 μm radius spherical silicon dome, placed on the other side of the antenna to attach the beam to the cable.

However, it was necessary to resize the structure geometry (antenna, substrate and lens) to meet the frequency band of Terabit DSL, from 0.1 to 0.3 THz [4].

Due to the radiation pattern of the original antenna used in [9], a reflective plane was inserted at the back of the substrate
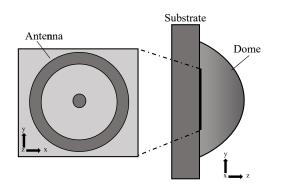
Fig. 5. Schematic representation of the antenna attached to the substrate and the coupling lens.

TABLE II
PARAMETERS OF THE ORIGINAL SIMULATED ANTENNA PROPOSED IN [9].

Parameters	Values[µm]
Inner electrode radius (r_i)	2.5
Gap radius (r_g)	102.5
External electrode radius (r_e)	112.5
Structure thickness (e)	0.035

as schematized in Fig. 6. This reflector plane was constructed using the PEC (Perfect Electric Conductor) material and aims to change the distant field pattern of the original antenna in free space, as shown in Fig. 7.
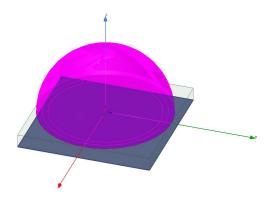

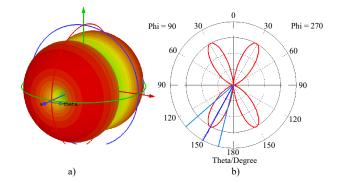Fig. 6. Dome, substrate and antenna with PEC on the back of the substrate.

Fig. 7. (a) Far-field of the antenna simulated at 0.3 THz in free space. (b) Antenna radiation pattern with radial polarization in the y-z plane at 0.3 THz.

2) Cable Positioning: To complete the scenario was necessary to define the waveguide position. In this article, the

waveguide used is a twisted-pair with characteristics of the CAT 5e (Enhanced Category 5), with the dimensions described in Table III based on the cross-section of the pair, as shown in Fig. 8.
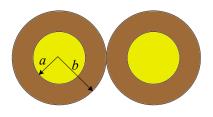

Fig. 8. Cross-section of twisted-pair.

TABLE III
CONSTRUCTIVE PARAMETERS OF THE TWISTED-PAIR.

Parameters	Value [mm]	Associated material
Conductor radius (a)	0.255	Copper
Insulation radius (b)	0.4	Polyethylene
Twist length	12.63	-x-

For the positioning of this twisted-pair in the scenario, it was evaluated which would be the best position, since in [9] this is not specified. Then, some positions were arbitrarily defined, and from the average signal power, it was determined which is the best position of the twisted-pair for the composition of the complete simulation scenario, as shown in Fig. 9.
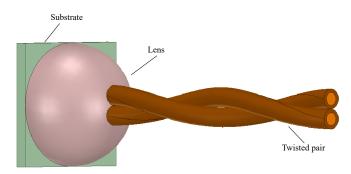

Fig. 9. Complete scenario design.

B. Coupling Evaluation and Guiding Analysis

The main objective of the article is to evaluate the coupling between the antenna and the twisted-pair. Coupling efficiency is the ratio between the power coupling on the twisted-pair and the power radiated by the antenna. Coupling efficiency is calculated by [17]:

$$\eta = \frac{P_{(avg,Pi)}}{P_{(avg,Po)}}, \tag{1}$$

where $P_{(avg,Pi)}$ is the power in the coupling plane and $P_{(avg,Po)}$ is the power in the output section of the antenna.

For the calculation of coupling efficiency, which is a power ratio, measurement sections were arranged to determine the average power in each plane, from the Eq. (2), as shown in Fig. 10. The measurement planes were defined as Po, Pi and Pf, which are the antenna output plane, coupling plane and
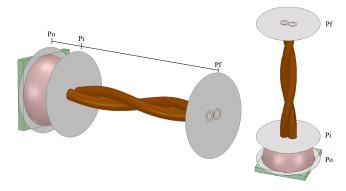
Fig. 10. Complete scenario design with measurement planes Po, Pi and Pf.

cable output plane, respectively. The average power, P_{avg}, in each plane is calculated as [12]:

$$P_{avg} = \frac{1}{2} \int_A \Re\{\vec{E} \times \vec{H}^*\} d\vec{A}, \qquad (2)$$

where $d\vec{A} = dA\hat{z}$, dA is the waveguide cross-section area element, $\vec{E}$ is the electric field and $\vec{H}^*$ is the conjugate of the magnetic field.

It is important to comment that the methodology adopted for calculating the average power and coupling efficiency was based on [17]. We consider that all the energy in the direction of propagation is coupled to the cable.

For guiding analysis in the cable, a power analysis is also performed in the measurement sections. However, instead of using the planes Po and Pi, the planes Pi and Pf are used, and it is possible to evaluate the decay in dB.

C. Calculating the Transmission Rate

After calculating the coupling efficiency, the channel rate predictions were calculated and compared with those predicted in [4]. This prediction was based on the Shannon's capacity compensated by the SNR (Signal to Noise Ratio) gap as [18]:

$$C = \Delta f \sum_{k=1}^{K} \log_2\left(1 + \frac{SNR_k}{\Gamma}\right), \qquad (3)$$

where the transmission rate C in bit/s is a function of the bandwidth of each subchannel Δf, the total number of subchannels K, the SNR in each subchannel SNR_k, and the SNR gap Γ, approximated by $\Gamma_{dB} \approx 9.75 + \gamma_m - \gamma_c$, where γ_c is the encoding gain and γ_m is the system margin desired, as defined for DSL systems [18]. In addition, the number of bits per subchannel is rounded to the nearest integer toward negative infinity and is limited to a maximum value.

The SNR per subchannel k is calculated by [18]:

$$SNR_k = \frac{|H_k|^2 p_k}{\sigma^2}, \qquad (4)$$

where the SNR depends on the absolute squared value of the transfer function of each mode $|H_k|^2$, the transmitter PSD (Power Spectral Density) p_k, the AWGN (Additive White Gaussian Noise) PSD σ^2. Using a flat transmitter PSD, the total transmit power, P_t, is divided equally for all subchannels in the frequency range. The absolute value of the transfer function for each mode is determined as [19]:

$$|H_k| = e^{-\alpha_k l}, \qquad (5)$$

where α_k is the attenuation constant of the mode over frequency of the subchannel k and l is the cable length in meters.

To consider the coupling on the rate predictions, the SNR should be calculated using the coupling efficiency in each subchannel, η_k, between the antenna and the twisted-pair, as defined by [18]:

$$SNR_k^{coupling} = \eta_k \frac{|H_k|^2 p_k}{\sigma^2}. \qquad (6)$$

Finally, the aggregate data rate achieved by the twisted-pair is determined as the sum of the capacity of each mode.

IV. RESULTS ANALYSIS

The scenario was gradually constructed and evaluated. First, the antenna was evaluated separately, the effects of the dome and substrate, and finally, the electromagnetic field behavior was evaluated in the complete scenario (antenna, dome, substrate and cable). Therefore, this section describes the results according to the evolution of the scenario, presenting as the main results the coupling between the antenna structure and cable, ending with a rate assessment based on the obtained coupling data.

A. Antenna Operation

The antenna model, as mentioned in Section III-A, was based on the article [9], it was simulated by varying some parameters for operation according to the Terabit DSL system, which uses a frequency range from 0.1 to 0.3 THz. Thus, the resonance frequency adjustment and improvement of the operating range were carried out from simulations varying the parameters below:

- Variation of the dimensions of the structure proportionally;
- Variation of port impedance;

Firstly, the antenna dimensions were varied, based on the configuration proposed in the base article and summarized in Table II, to adjust the frequency range of the Terabit DSL scenario. The variation was made by multiplying all dimensions by a constant m. The constant m was varied until the desired frequency range was reached. For this, in the simulations performed, the values of 1, 2, 5, 8, 11, 14, 17, and 20 were adopted for m. The most appropriate value of m for the range of interest was 20, as can be seen in Fig. 11, where the S_{11} decays significantly from 0.1 THz, as desired.

To estimate the antenna impedance to $m = 20$, the scattering parameter was used as a metric while the port impedance was varied. The smaller the scattering parameter, the port impedance got closer to the antenna impedance. Then, in the software HFSS, a variation of the impedance value was carried out from the default value of the software, 50 Ω, until the impedance value where the level of the scattering parameter
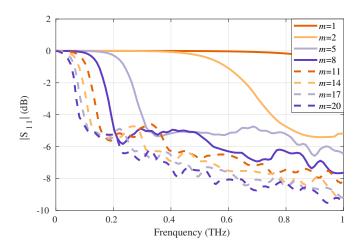
Fig. 11. Behavior of scattering parameter in function of frequency range from variation of dimension of antenna, considering the values of *m* equal 1, 2, 5, 8, 11, 14, 17, and 20.

became appropriate, e.g. defined in [20] equal to or less than -10 dB.

In Fig. 12, it is possible to notice that the impedance variation does not change the operating frequency range, as it happened with the dimension variation, but change the level of the parameter $|S_{11}|$. As this parameter was changed, the $|S_{11}|$ curve reached levels below -10 dB. Fig. 12 shows that over the impedance variation the most suitable value is around 150 Ω, this behavior is confirmed by observing the levels of the parameter $|S_{11}|$ that for smaller and greater values than 150 Ω are at levels above -10 dB. Then, it is determined that the antenna impedance is approximately 150 Ω.

Starting from the frequency determination, with the parameter *m* chosen equal to 20 and with the appropriate levels of $|S_{11}|$ for propagation, the antenna used for the next simulations will have new dimensions: internal electrode radius, r_i, 50 μm, gap radius, r_g, 2.05 mm and external electrode radius, r_e, 2.25 mm.
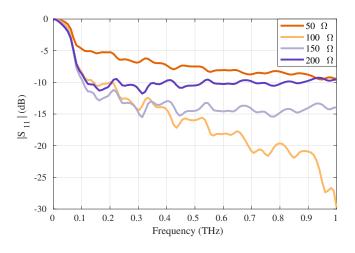

Fig. 12. Impedance variation according to the appropriate size of the antenna (*m*=20) showing changes in $|S_{11}|$ parameter level.

B. Substrate and Lens Adaptation

As the dimensions of the antenna were changed, the dimensions of the substrate and the lens became disproportionate. Then, an evaluation was made to choose the most suitable dimension for these structures, according to the new dimension of the antenna.

In this analysis, a constant *n* was defined, in the same way as the constant *m*, to vary proportionally the dimensions of the lens and substrate. In order to evaluated which value of *n* was more appropriate, an average power measurement section was placed at the lens output and verified which returned the highest value, as shown in Fig. 13.

The constant *n* was defined starting from a value in which the antenna's entire structure was included in the substrate and lens structures. The value 1 was not chosen because the antenna would still be at the edge of the structure. So, the variation started from 1.1, slightly higher than the antenna structure, up to 2.
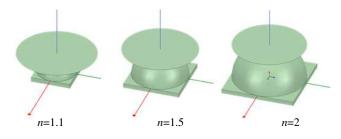

Fig. 13. Variation in the dimension of the dome and substrate structures according to the parameter *n*.

The results of average power in the lens output section, presented in Table IV, obtained in the simulations, indicate that among the investigated values the most suitable dimension for the lens and substrate was *n* equal to 1.1. The dimension of *n* equal to 1.1 was chosen because it reached the highest average power value, 0.6018, and concentrated more the field in the section, as is clearly observed in Fig. 14.
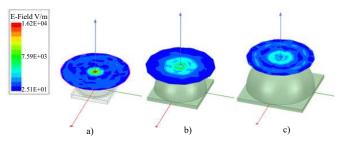

Fig. 14. Planes for measuring field concentration for different dimensions of *n*. a) *n* = 1.1 b) *n* = 1.5 c) *n* = 2.

From these results, the new dimensions of the dome radius and substrate width were 2.475 mm and 4.95 mm, respectively. The radius of the dome and the width of the substrate were changed according to the variation of *n*, but the thickness of the substrate was maintained.

With this determined dimension and with the insertion of the PEC in the back part of the substrate, it was possible to evaluate the far-field of the structure and radiation diagram, presented in Fig. 15.

TABLE IV
AVERAGE POWER IN OUTPUT SECTION FOR PARAMETER VARIATION n.

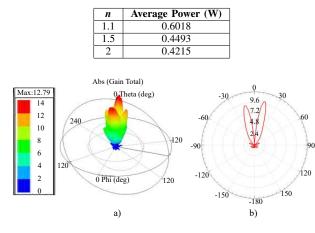| n	Average Power (W)
1.1	0.6018
1.5	0.4493
2	0.4215

Fig. 15. a) Far-field and b) radiation diagram of the antenna with dome, substrate and PEC at the back of the substrate.

It can be seen in Fig. 15 that the electromagnetic field distribution, far-field, and the radiation diagram in Fig. 15b of the structure maintained their radial configuration but only directed on the axis positive z.

C. Positioning of Twisted-Pair

In order to complete the setting of the scenario, it was necessary to evaluate in which position the twisted-pair should be placed. For this, the position was varied along the z axis, with some positions defined: inside the dome $(x, y, z) = (0, 0, 0.1)$ and $(x, y, z) = (0, 0, 1.275)$, at the exit of the dome $(x, y, z) = (0, 0, 2.475)$ and away from the dome $(x, y, z) = (0, 0, 3.5)$ and $(x, y, z) = (0, 0, 4.5)$.

For this evaluation, the average power was measured in the coupling section, Pi, and in the cable exit section, Pf, checking which position reached the best values. This variation was done until the average power value started to decrease, as it happened with the power value for the last position of z. The results obtained in this evaluation are presented in Table V.

TABLE V
AVERAGE POWER IN SECTION Pi AND Pf FOR DIFFERENT CABLE POSITIONS.

Position (mm)	Avg. power at Pi(W)	Avg. power at Pf(W)
z = 0.1	0.5547	0.0531
z = 1.2375	0.3272	0.0600
z = 2.475	0.3280	0.0971
z = 3.5	0.3655	0.1132
z = 4.5	0.3602	0.0804

From these results, it was defined that the best position for the twisted-pair is (x,y,z) = (0,0,3.5), since it was the value that reached the highest average power in the measurement section. As shown in Table V, the field guidance did not happen, although some positions have high values in Pi, demonstrating that the power calculated in the section was not exactly that coupled to the cable, as for example in $z = 0.1$.

D. Coupling Evaluation

After the complete adjustment of the scenario, with the proper positioning of the cable, it was possible to evaluate the signal coupling between the antenna and the twisted-pair. The coupling was calculated for the central frequency of Terabit DSL, 0.2 THz, from Eq. (1) and Eq. (2), as explained in the Section III-B.

Thus, the coupling was calculated from Eq. (1) using the average power values in the Po and Pi sections. The average power values in the sections were 0.657 W and 0.365 W, so the coupling between the antenna and the twisted-pair cable was 55.57 %, at 0.2 THz. The electromagnetic field in the Po and Pi sections can be observed in Fig. 16.
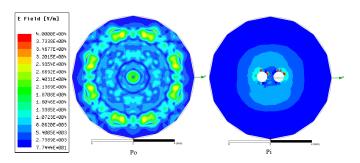

Fig. 16. Electromagnetic field in measuring planes Po and Pi.

In addition to calculating the coupling at the center frequency of the Terabit DSL, 0.2 THz, the coupling was calculated over the entire frequency range of the system, which will assist in the prediction of the transmission rate. The results are shown in Fig. 17.
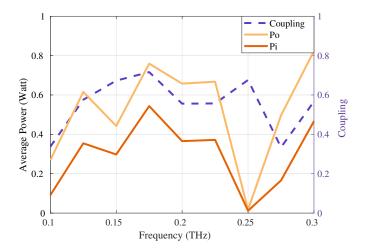

Fig. 17. Average power in the Po and Pi planes and coupling, for antenna with new defined dimensions in 0.2 THz.

From the analysis of Fig. 17, it is possible to notice that the coupling in the twisted-pair is quite variable as the frequency also varies. This variation reaches levels below 40% up to values of 71.62% in the frequency of 0.175 THz, in addition to intermediate values of for example 55.57% in the frequency of 0.2 THz.

It is important to note that despite the coupling values being at levels above 50 %, in some points the average power
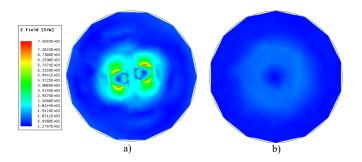
Fig. 18. Electromagnetic field in the Pf planes. a) With cable and b) Without cable.

value is extremely low, such as 0.25 THz. The exact reason for this power drop at this frequency point cannot be stated, but a potential reason would be that the field reflected by the reflective surface would destructively interfere in the field emitted to the twisted-pair. So, in a real transmission it would be interesting to evaluate an antenna that obtains powers at appropriate levels in the entire frequency band, or else use the simulated antenna only for frequency bands with adequate powers.

Although the coupling presented high values, one question that needed to be discussed was whether this energy was being guided by the cable or was only following the direction of propagation of the positive z-axis. Thus, we performed a simulation of the complete scenario (antenna, substrate, lens and cable) and one of the scenario without the cable (antenna, substrate and lens) and positioned a measurement section in the P_f position, position shown in the Fig. 10, for both cases.

As a result of this evaluation, Fig. 18, shows the measurement section at position Pf, showing that, in addition to the efficient coupling on the twisted-pair cable, the energy is guided along the z-axis. In Fig. 18b it is clear to see that without the cable the power disperses before reaching the measurement section (Pf), while in Fig. 18a, the field is guided in the vicinity of the cable.

E. Prediction of Transmission Rate

The system transmission rate is calculated using the methods described in Section III-C, considering the attenuation results of the higher-order modes of the twisted-pair in Fig. 2 and the coupling between a radial antenna and the twisted-pair presented in Fig. 17. Some necessary parameters for calculating the rate are described in Table VI and were all taken from [4]. As the attenuation and coupling efficiency were simulated with fewer points than the number of subchannels, an interpolation was made to obtain them with the same number of frequency points.

It is important to say that to aggregate the rates of each propagation mode, it is necessary to design a specific antenna for each mode. In general, each of these antennas would have its own characteristics and different coupling coefficients. In this work, for simplicity, we consider that the radial antenna excites all four guided modes of Fig. 2 and the coupling efficiency obtained in Fig. 17 is considered to be the same for each one.

TABLE VI
PARAMETERS USED TO CALCULATE THE RATE.

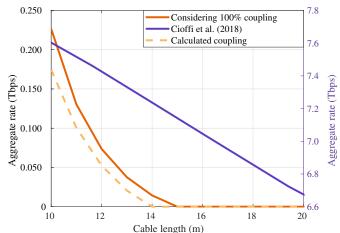| Parameters	Value
Number of subchannels (K)	4096
Maximum of bits per subchannel	12
Codification gain (γ_c)	7.0 dB
Margin (γ_m)	6.0 dB
Total transmit power per mode (P_t)	20 dBm
Spectral power density σ^2 do AWGN	-160 dBm/Hz

Fig. 19. Comparison of the predicted rate of this article (Calculated coupling) and that predicted in the literature, considering 100% coupling and the rate predicted by Cioffi in [4].

Fig. 19 shows the aggregate bit rate versus the cable length variation for the proposed radial antenna structure by considering the frequency range of 0.1 to 0.3 THz. For comparison, the figure also shows the same results considering 100 % coupling and the predicted rate from Cioffi et al. [4].

It was observed from the rate provided in Fig. 19, that the levels provided in [4] really are overestimated, as expected due to the simple electromagnetic model that was assumed for the twisted-pair. It is also shown that the rate is slightly below the rate that considers a coupling ideal (100 %) between the antenna and the modes excited in the cable. For a cable with a length of 10 meters, the aggregate rate to the user is around 0.17 Tbps, while for 100 % coupling it reaches values of 0.24 Tbps and in [4] exceeds 7 Tbps.

As for the results in [8], the data rates above 1 Tbps are achievable at short distances, approximately below 10 m, and reach about 30 Gbps at 15 m. This is much more similar to our results, however, the cable measured in [8] does not have the typical characteristics of a twisted-pair, such as its twisting and isolation, making it difficult to compare with ours results for a twisted-pair.

Fig. 20 evaluates which modes enable data transmission using the coupling provided by the proposed radial antenna structure for different twisted-pair lengths, i.e., 1, 5 and 10 meters. According to this figure, it is possible to transmit in the 4 modes of the considered twisted-pair from 1 and 5 meters, but in 10 meters, the attenuation levels of the 1st and 3rd modes are very high, and only the 2nd and 4th modes can be used.
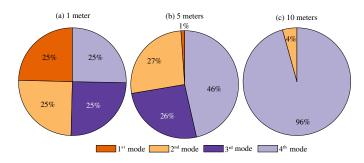
Fig. 20. Contributions of the higher-order modes to the aggregate data rate.

V. CONCLUSION

This article investigated the signal coupling between a twisted-pair and a radially propagated antenna, in the frequency range of the Terabit DSL system. These systems have recently been suggested to operate at Terabit rates per second, as an evolution to DSL technology. However, a challenge of this technology is the coupling of these guided modes in the twisted-pair. The analyses of this article are based on numerical simulations about the coupling efficiency between an antenna with radial propagation and a twisted-pair, in a frequency of 0.1 to 0.3 THz. As a result, this article shows 55.57 % coupling efficiency in the central frequency of the band and reaching levels of up to 71.62 % for the frequency of 0.175 THz. From the coupling results, the rate forecasts were calculated reaching levels of 0.17 Tbps for twisted-pairs up to 10 meters, showing that some data in the literature are unrealistic since they do not consider real scenarios. Future works should also design specific antennas to couple into the higher-order modes of twisted-pairs. Taking into account that the field distribution of each mode may not have radial symmetry, future works should also investigate the use of broadband antennas with linear (bow-tie) or circular (log-spiral) polarization.

REFERENCES

[1] "Multi-gigabit fast access to subscriber terminals (mgfast) - phy," ITU-T recommendation, October 2018. [Online]. Available: https://www.itu.int/md/T17-SG15-181008-TD-WP1-0258

[2] W. Coomans, R. B. Moraes, K. Hooghe, A. Duque, J. Galaro, M. Timmers, A. J. van Wijngaarden, M. Guenach, and J. Maes, "XG-fast: the 5th generation broadband," *IEEE Communications Magazine*, vol. 53, no. 12, pp. 83–88, December 2015, doi: 10.1109/MCOM.2015.7355589.

[3] P. Öhlén, B. Skubic, A. Rostami, K. Laraqui, F. Cavaliere, B. Varga, and N. F. Lindqvist, "Flexibility in 5G transport networks: The key to meeting the demand for connectivity," October 2015, ericsson Technology Review. [Online]. Available: https://www.ericsson.com/en/reports-and-papers/ericsson-technology-review/articles/flexibility-in-5g-transport-networks-the-key-to-meeting-the-demand-for-connectivity

[4] J. M. Cioffi, K. J. Kerpez, C. S. Hwang, and I. Kanellakopoulos, "Terabit DSLs," *IEEE Communications Magazine*, vol. 56, no. 11, pp. 152–159, November 2018, doi: 10.1109/MCOM.2018.1800597.

[5] Y. Leviatan and A. Adams, "The response of a two-wire transmission line to incident field and voltage excitation, including the effects of higher order modes," *IEEE Transactions on Antennas and Propagation*, vol. 30, no. 5, pp. 998–1003, September 1982, doi: 10.1109/TAP.1982.1142893.

[6] D. D. Souza, B. Sousa, G. Borges, R. M. Rodrigues, A. M. Cavalcante, I. Almeida, and J. Weyl Costa, "Evaluation of copper cables as waveguides in next-generation wireline technologies," in *SBMO/IEEE MTT-S International Microwave and Optoelectronics Conference (IMOC) (IMOC'2019)*, Aveiro, Portugal, November 2019.

[7] R. Shrestha, K. Kerpez, C. S. Hwang, M. Mohseni, J. Cioffi, and D. M. Mittleman, "A metal wire waveguide for terabit DSL," in *44th International Conference on Infrared, Millimeter, and Terahertz Waves (IRMMW-THz)*, September 2019, pp. 1–2, doi: 10.1109/IRMMW-THz.2019.8873828.

[8] R. Shrestha, K. Kerpez, C. S. Hwang, M. Mohseni, J. M. Cioffi, and D. M. Mittleman, "A wire waveguide channel for terabit-per-second links," *Applied Physics Letters*, vol. 116, no. 13, p. 131102, March 2020, doi: 10.1063/1.5143699.

[9] J. A. Deibel, K. Wang, M. D. Escarra, and D. M. Mittleman, "Enhanced coupling of terahertz radiation to cylindrical wire waveguides," *Optics Express*, vol. 14, no. 1, pp. 279–290, January 2006, doi: 10.1364/OPEX.14.000279.

[10] T. K. Sarkar, M. N. Abdallah, M. Salazar-Palma, and W. M. Dyab, "Surface plasmons-polaritons, surface waves, and zenneck waves: Clarification of the terms and a description of the concepts and their evolution." *IEEE Antennas and Propagation Magazine*, vol. 59, no. 3, pp. 77–93, June 2017, doi: 10.1109/MAP.2017.2686079.

[11] R. E. Collin, *Surface Waveguides*. in Field Theory of Guided Waves, 1991, doi: 10.1109/9780470544648.ch11.

[12] S. J. Orfanidis, *Electromagnetic waves and antennas*. Rutgers University New Brunswick, NJ, 2016. [Online]. Available: http://www.ece.rutgers.edu/~orfanidi/ewa

[13] A. Bur, "Dielectric properties of polymer at microwave frequencies," *Polymer*, vol. 26, p. 963, September 1985, doi: 10.1016/0032-3861(85)90216-2.

[14] K. Wang and D. M. Mittleman, "Metal wires for terahertz wave guiding," *Nature*, vol. 432, no. 7015, pp. 376–379, November 2004, doi: https://doi.org/10.1038/nature03040.

[15] L. Chusseau and J.-P. Guillet, "Coupling and propagation of sommerfeld waves at 100 and 300 GHz," *Journal of Infrared, Millimeter, and Terahertz Waves*, vol. 33, pp. 174–182, February 2012, doi: 10.1007/s10762-011-9854-x.

[16] A. Agrawal and A. Nahata, "Coupling terahertz radiation onto a metal wire using a subwavelength coaxial aperture," *Optics Express*, vol. 15, pp. 9022–8, August 2007, doi: 10.1364/OE.15.009022.

[17] Z. Zheng, N. Kanda, K. Konishi, and M. Kuwata-Gonokami, "Efficient coupling of propagating broadband terahertz radial beams to metal wires," *Optics Express*, vol. 21, no. 9, pp. 10 642–10 650, May 2013, doi: 10.1364/OE.21.010642.

[18] T. Starr, M. Sorbara, J. Cioffi, and P. Silverman, *DSL Advances*, ser. Prentice Hall Communications E. Prentice Hall PTR, 2003. [Online]. Available: https://books.google.com.br/books?id=evNSAAAAMAAJ

[19] P. Golden, H. Dedieu, and K. Jacobsen, *Fundamentals of DSL Technology*. CRC Press, 2005. [Online]. Available: https://books.google.com.br/books?id=m77kZl71gysC

[20] N. Dolatsha, B. Grave, M. Sawaby, C. Chen, A. Babveyh, S. Kananian, A. Bisognin, C. Luxey, F. Gianesello, J. Costa, C. Fernandes, and A. Arbabian, "17.8 a compact 130 GHz fully packaged point-to-point wireless system with 3D-printed 26 dBi lens antenna achieving 12.5 Gb/s at 1.55pJ/b/m," in *IEEE International Solid-State Circuits Conference (ISSCC)*, February 2017, pp. 306–307, doi: 10.1109/ISSCC.2017.7870383.

Brenda Penedo Tavares de Sousa received a B.Sc. in Electrical Engineering in 2018 from the Federal University of Pará (UFPA), Spc. in energy efficiency and energy quality in 2019 from amazon energy efficiency excellence center (CEAMAZON), and a M.Sc. in electrical engineering with emphasis on telecommunication in 2020 from UFPA, Belém, Brazil, where she is currently pursuing a Ph.D. She is currently part of the research team of the applied electromagnetism laboratory (LEA) in partnership with Ericsson. Has experience in wired communications, Transmission modes in DSL systems and Coupling and propagating guided modes on twisted-pair cables.

Daynara Dias Souza received a B.Sc. in electrical engineering, in 2018, and an M.Sc. in electrical engineering with emphasis on telecommunication, in 2020, from Federal University of Pará (UFPA), Belém, Brazil, where she is currently working toward the Ph.D. degree. She has experience in broadband communication systems. Her current research topic is resource allocation for wireless communication systems.

Gilvan Soares Borges received degrees as an engineer, M.Sc. and Ph.D. in electrical engineering from the Federal University of Pará (UFPA) in the years 2007, 2010 and 2016, respectively. He is currently a professor at the Federal Institute of Education, Science and Technology of Pará (IFPA). Among his areas of interest are applied electromagnetism, computational intelligence and broadband communication systems.

Roberto Menezes Rodrigues received the Ph.D. degree in electrical engineering in 2012 from the Federal University of Pará (UFPA), Belém, Brazil. Currently, he is a professor of the Electrical and Biomedical Engineering Faculty at UFPA. He is also affiliated to the Applied Electromagnetism Laboratory (LEA). His current research interests are 5G networks, energy harvesting, and swarm robotics.

André Mendes Cavalcante received his Ph.D. on Electrical Engineering from Federal University of Pará (UFPA), Brazil, in 2007. From 2007 to beginning of 2016, he was coworker at Nokia Institute of Technology (INDT), Brazil, where he was engaged in several R&D projects related to wireless communications. Currently, he is a Senior Researcher at Ericsson Research, Brazil. His main research topic is mobile transport network for future wireless communication systems.

João C. Weyl Albuquerque Costa (S'94–M'95) received a B.Sc. in electrical engineering from the Federal University of Pará (UFPA), Belém, Brazil, in 1981, an M.Sc. in electrical engineering from the Pontifical Catholic University of Rio de Janeiro, Rio de Janeiro, Brazil, in 1989, and a Ph.D. in electrical engineering from the State University of Campinas, Campinas, Brazil, in 1994. He is currently a professor with the Institute of Technology, UFPA, and a researcher with the Brazilian Research Funding Agency National Council for Scientific and Technological Development, Brasília, Brazil. His current research interests include broadband systems and optical sensors.